Pulse of atmospheric oxygen during the late Cambrian

Matthew R. Saltzman[a,1], Seth A. Young[b], Lee R. Kump[c], Benjamin C. Gill[d,e], Timothy W. Lyons[e], and Bruce Runnegar[f]

[a]School of Earth Sciences, Ohio State University, Columbus, OH 43210; [b]Department of Geological Sciences, Indiana University, Bloomington, IN 47405; [c]Department of Geosciences and Astrobiology Research Center, Pennsylvania State University, University Park, PA 16802; [d]Department of Earth Sciences, University of California, Riverside, CA 92521; [e]Department of Earth and Planetary Sciences, Harvard University, Cambridge, MA 02138; and [f]Department of Earth and Space Sciences and Institute of Geophysics and Planetary Physics, University of California, Los Angeles, CA 90095

Edited* by Robert A. Berner, Yale University, New Haven, CT 06520, and approved January 20, 2011 (received for review August 19, 2010)

A rise in atmospheric O_2 has been linked to the Cambrian explosion of life. For the plankton and animal radiation that began some 40 million yr later and continued through much of the Ordovician (Great Ordovician Biodiversification Event), the search for an environmental trigger(s) has remained elusive. Here we present a carbon and sulfur isotope mass balance model for the latest Cambrian time interval spanning the globally recognized Steptoean Positive Carbon Isotope Excursion (SPICE) that indicates a major increase in atmospheric O_2. We estimate that this organic carbon and pyrite burial event added approximately 19×10^{18} moles of O_2 to the atmosphere (i.e., equal to change from an initial starting point for O_2 between 10–18% to a peak of 20–28% O_2) beginning at approximately 500 million years. We further report on new paired carbon isotope results from carbonate and organic matter through the SPICE in North America, Australia, and China that reveal an approximately 2‰ increase in biological fractionation, also consistent with a major increase in atmospheric O_2. The SPICE is followed by an increase in plankton diversity that may relate to changes in macro- and micronutrient abundances in increasingly oxic marine environments, representing a critical initial step in the trophic chain. Ecologically diverse plankton groups could provide new food sources for an animal biota expanding into progressively more ventilated marine habitats during the Ordovician, ultimately establishing complex ecosystems that are a hallmark of the Great Ordovician Biodiversification Event.

evolution | climate change | stable isotope | Paleozoic | dinoflagellate

Fluctuations in atmospheric oxygen (O_2) and oceanic redox are thought to have played fundamental roles in driving biological evolution throughout geologic time (1, 2). Well-studied examples include the rise of animals at the end of the Precambrian eon (3) and the rise of modern phytoplankton groups in the early Mesozoic (4), both of which have been linked to increases in atmospheric O_2. Rising oxygen levels may directly influence nutrient availability for phytoplankton or animal physiology, with subsequent biological feedbacks between the benthos and plankton leading to increased ecological complexity (5–7). Here we document a significant increase in atmospheric O_2 during the later Cambrian and examine the impact this may have had on biological evolution.

Beginning in the later parts of the Cambrian and continuing through much of the Ordovician, a series of complex, diachronous episodes of both plankton and animal diversification are collectively referred to as the Great Ordovician Biodiversification Event (GOBE), or Ordovician radiation (8–10). Although ecological interaction between free-floating (planktic) and bottom-dwelling (benthic) organisms has been recognized as major driver of biological evolution during this time period (11, 12), changes in the physical environment were likely an important stimulus. Specifically, previous authors have proposed that increased nutrient availability could fuel increases in primary productivity and food resources during the GOBE. However, potential mechanisms to drive enhanced productivity and associated trophic changes remain poorly understood (12, 13). The unique evidence we present here for a later Cambrian (Furongian Series) rise in atmospheric O_2 may have altered oceanic redox and the concentrations of bioavailable nutrients in the surface oceans, ultimately promoting diversification in certain phytoplankton groups and potentially higher overall net primary production as well.

Late Cambrian changes in the oceanic trophic chain ("plankton revolution" of Servais et al.) (12) began in the aftermath of a major perturbation in the global carbon cycle that is recorded in the geologic record as a large positive $\delta^{13}C_{carb}$ excursion [Steptoean Positive Carbon Isotope Excursion (SPICE) event] (14) (Fig. 1). The SPICE event has been documented worldwide and is characterized by a positive $\delta^{13}C$ shift of approximately +4‰ in Upper Cambrian (Paibian Stage of Furongian Series) sections throughout North America and time-equivalent strata in China, Siberia, Baltica, Australia, and Kazakhstan (refs. 14–16, Fig. S1, and *SI Text*). Intercontinental correlation of the SPICE is based on the presence of cosmopolitan trilobite *Glyptagnostus reticulatus* below the $\delta^{13}C$ peak and *Irvingella* above. The SPICE was also associated with an approximately +20‰ increase in the $^{34}S/^{32}S$ ratio of seawater sulfate as measured in carbonate-associated sulfate ($\delta^{34}S_{CAS}$) (Fig. 1) and likely represents an interval of enhanced organic carbon and pyrite sulfur beneath anoxic (euxinic) waters (17). The positive $\delta^{13}C_{carb}$ and $\delta^{34}S_{CAS}$ excursions, which lasted for several million years based on the best absolute age constraints for the Cambrian (14), should have been associated with significant net O_2 production. Here we show that a rise in atmospheric O_2 occurred during the SPICE using two different methods. First, we utilize a conventional carbon-sulfur isotope mass balance approach that is based on published $\delta^{13}C_{carb}$ and $\delta^{34}S_{CAS}$ measurements (18, 19). Second, we present unique paired analyses of carbonates ($\delta^{13}C_{carb}$) and organic matter ($\delta^{13}C_{org}$) in three global sections through the SPICE to consider an O_2 proxy that is based on changes in biological fractionation of carbon isotopes (20, 21).

Results and Discussion

Carbon and Sulfur Isotope Mass Balance. Calculations of atmospheric O_2 levels through geologic time can be made using global estimates of the burial and weathering rates of organic carbon and pyrite sulfur in sedimentary rocks (18, 19). The isotope mass balance approach utilizes secular trends in the stable isotope ratios of carbon ($\delta^{13}C_{carb}$) and sulfur ($\delta^{34}S_{CAS}$) in marine minerals. Because photosynthesis and bacterial sulfate reduction discriminate in favor of the light isotopes of carbon (^{12}C) and sulfur (^{32}S),

Author contributions: M.R.S. and L.R.K. designed research; M.R.S., S.A.Y., L.R.K., B.C.G., T.W.L., and B.R. performed research; M.R.S., S.A.Y., L.R.K., B.C.G., and T.W.L. analyzed data; and M.R.S. and L.R.K. wrote the paper.

The authors declare no conflict of interest.

*This Direct Submission article had a prearranged editor.

[1]To whom correspondence should be addressed. E-mail: saltzman.11@osu.edu.

This article contains supporting information online at www.pnas.org/lookup/suppl/doi:10.1073/pnas.1011836108/-/DCSupplemental.

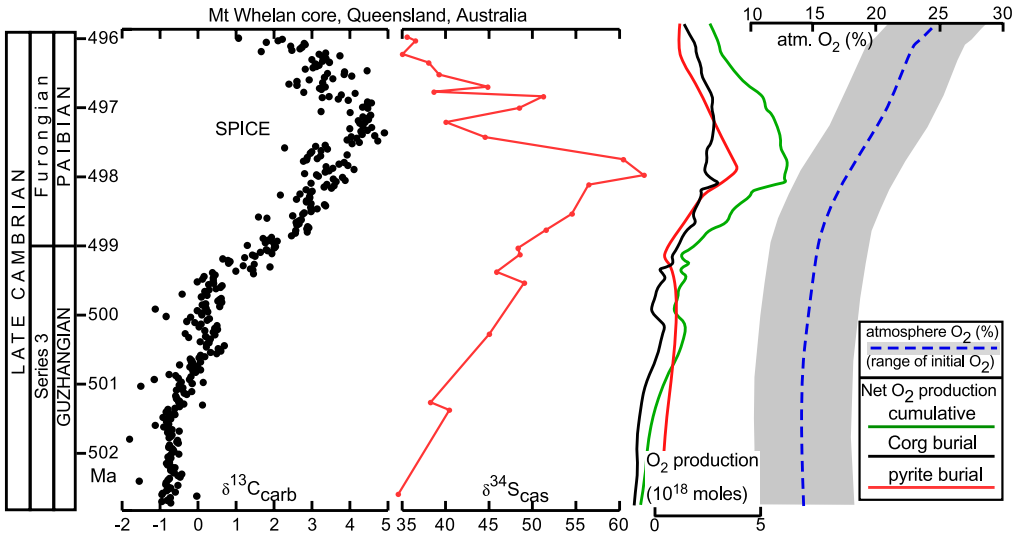

Fig. 1. Plot of $\delta^{13}C_{carb}$ (14) and $\delta^{34}S_{CAS}$ (17) data from Mt. Whelan core in Australia that were used in the isotope mass balance model (see Table S1) to calculate changes in atmospheric O_2. Lines shown to right of data indicate net O_2 production by organic carbon and pyrite burial, as well as total O_2(in units of 10^{18} moles). Note that the model begins out of steady-state with a small net O_2 sink due to the initial Corg burial rate being less than the initial Corg weathering rate (see text for discussion). The cumulative atmospheric O_2 production of approximately 19×10^{18} moles would have increased an atmosphere initially containing approximately 18% O_2 (from Berner's GEOCARBSULF model) (19) to near 28%. The shaded area for the trend in % O_2 encompasses an initial lower boundary for the starting point of 10.5% O_2 and a median (dashed line) starting point of about 14%. It is possible, however, that the initial O_2 level may have been even lower (approximately 5% in Bergman et al. COPSE model) (23).

the oceans become isotopically heavier as net burial rates of organic carbon and pyrite sulfur increase.

We used a carbon and sulfur isotope mass balance model to calculate the pO_2 increase during the late Cambrian SPICE event based on the approach of Kurtz et al. (22) developed for their analysis of Cenozoic C and S coupling. The model relies on relatively high-resolution carbon and sulfur isotope records to calculate burial fluxes of pyrite and organic carbon with no required assumption of steady state (ref. 22; their equations 4 a and b). The weathering fluxes, isotopic compositions, and pyrite sulfur weathering proportions are held constant by assuming an initial steady state (see Table S1). The weathering fluxes, isotopic compositions, and organic carbon weathering proportions are held constant by assuming steady state at the canonical value of $\delta^{13}C_{carb} = 0‰$ (see Table S1 and ref. 18), which occurs at about 2 million yr (my) into the SPICE. Thus, we begin the model out of steady state with a net O_2 sink (i.e., O_2 declining) due to the initial Corg burial rate (3.7×10^{18} moles C/my) being less than the initial Corg weathering rate (4.6×10^{18} moles C/my).

The variations in isotopic fractionation documented here are used for $\delta^{13}C$ in the model but a constant fractionation of 35‰ is used for $\delta^{34}S$ (ref. 22, although see ref. 17 for a discussion of variable sulfur fractionation). The C content of the ocean/atmosphere system is held constant (at the modern, steady-state value), but the S content of the ocean is allowed to evolve (with a fixed gypsum deposition rate) (Table S1). As a result, the sulfate content of the ocean is initially set at 1.5 mmol kg^{-1}, about 5% of modern (see ref. 17 for discussion), and falls by about 50% during the course of the simulation. An evolution of atmospheric O_2 contents is determined based on an initial oxygen value (19) and the organic carbon and pyrite fluxes determined through isotope balance.

The mass balance model uses $\delta^{13}C_{carb}$ and $\delta^{34}S_{CAS}$ data from the Mt. Whelan core in Australia (Fig. 1). Solving for the burial fluxes requires both the isotopic records and their first derivatives (22). Because any noise in the two isotopic datasets will be amplified in the derivative curve, we first smoothed the $\delta^{13}C_{carb}$ and $\delta^{34}S_{CAS}$ records using cubic smoothing splines (22). The smoothed curves represent a visual best fit to the data (Fig. 1) and preserve the important features of the timing and magnitude of observed excursions.

The net atmospheric O_2 production through the SPICE event includes significant contributions from both organic carbon and pyrite burial (Fig. 1), with a cumulative production of approximately 19×10^{18} moles. Most of the O_2 production occurred during a 2-million-year time period centered on the peak of the SPICE (Fig. 1), during which time organic carbon burial rates were elevated above steady state at approximately 7×10^{18} moles C/my and non-steady-state pyrite burial rates were approximately 3×10^{18} moles S/my. The cumulative atmospheric O_2 production of approximately 19×10^{18} moles would have increased an atmosphere initially containing approximately 18% O_2 (from Berner's GEOCARBSULF model) (19) to near 28% (Fig. 1), although the initial O_2 level may have been lower (approximately 5% in Bergman et al. COPSE model) (23, 24). Regardless of peak levels achieved (for comparison, current atmosphere O_2 is 21%), atmospheric O_2 stabilizes at this new, higher steady-state value at the end of the model run as $\delta^{13}C_{carb}$ and $\delta^{34}S_{CAS}$ fall to approximately their preexcursion ratios.

O_2-Dependent Carbon Isotope Fractionation. Based on the carbon and sulfur isotope mass balance model discussed above, we can argue with confidence that a significant rise in pO_2 took place during the SPICE due to elevated rates of organic carbon and pyrite burial. As a test of this predicted rise in pO_2, we compare the timing and net production estimated from our isotope mass balance model with O_2 proxy records based on $\Delta^{13}C$ calculated from paired analysis of $\delta^{13}C_{carb}$ and $\delta^{13}C_{org}$ (20, 21).

We have measured $\delta^{13}C_{org}$ in carbonate rocks for three regions in which the SPICE $\delta^{13}C_{carb}$ excursion is already well documented (Fig. 2; see refs. 14 and 25, Fig. S1, and *SI Text* for descriptions of individual sections). To be confident in our evaluation of temporal changes in the isotopic offset (fractionation) between inorganic and organic carbon (26), we compared $\delta^{13}C_{carb}$ and $\delta^{13}C_{org}$ data from the same sample. In all three study areas—using drill core samples from Iowa (United States), and Queensland (Australia) and fresh outcrop material from Hunan (China) (Fig. S1)—the $\delta^{13}C_{org}$ curve initially tracks the $\delta^{13}C_{carb}$ shift to heavier values in the lower portion of the SPICE (Fig. 2). How-

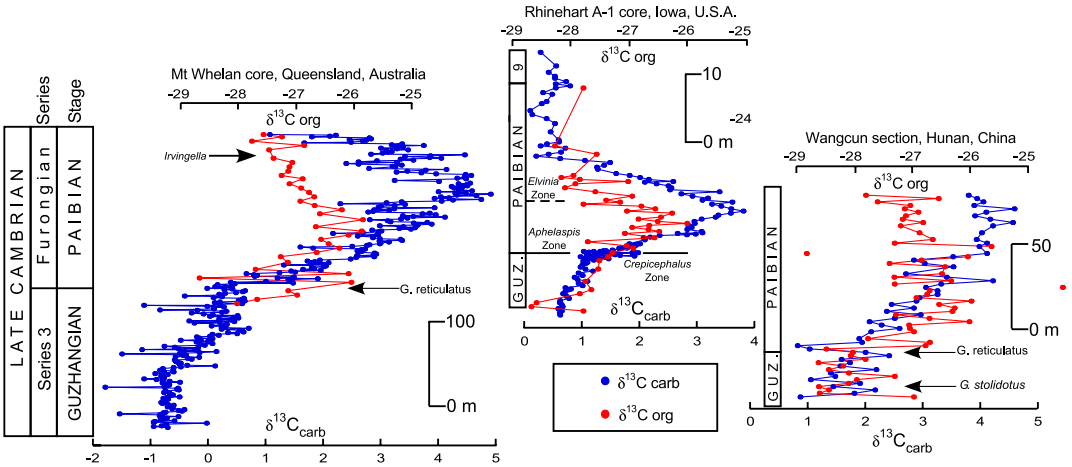

Fig. 2. Plot of $\delta^{13}C_{carb}$ and $\delta^{13}C_{org}$ (‰ VPDB) through the Late Cambrian SPICE excursion. Cosmopolitan trilobite taxa allowing for global correlation are indicated with arrows (Australia, China), and North American trilobite zones that correlate are shown for Iowa (refs. 14 and 25; Figs. S1 and S2; Tables S2, S3, and S4; and *SI Text*).

ever, part way through the rising limb of the $\delta^{13}C_{carb}$ excursion, the $\delta^{13}C_{org}$ values begin to decrease, yielding an increase in the isotopic difference between paired $\delta^{13}C_{org}$ and $\delta^{13}C_{carb}$ ($\Delta^{13}C$) data from ~28 and 29‰ before the SPICE to a peak of 31‰ at the height of the excursion followed by a return to preexcursion values after the SPICE (Fig. 3).

The dependence of biological carbon isotope fractionation on the partial pressure of atmospheric oxygen (pO_2) has been demonstrated in laboratory experiments using vascular land plants, bryophytes, and marine phytoplankton (20, 21, 27). Increased isotopic discrimination for ^{12}C is observed at increasing O_2 levels because CO_2 levels rise within the plant or plankton cell as photorespiration begins to outpace photosynthesis (O_2 competes with CO_2 for sites on the photosynthetic enzyme Rubisco).

We modified equation 4 in Beerling et al. (21) to calculate O_2 from our measured $\delta^{13}C_{carb}$ and $^{13}C_{org}$ values: $\Delta^{13}C_{meas} = \Delta^{13}C_{initial} + J \times [(M_{O2}/38) - 1]$. The term $\Delta^{13}C_{meas}$ is the measured value for the difference between $\delta^{13}C_{carb}$ and $^{13}C_{org}$ and $\Delta^{13}C_{initial}$ is an estimate of the Early Paleozoic baseline value (approximately 29‰) (19). We use a value of $J = 5$ in our calculations, based on the best fit to both the experimental data for isotopic discrimination in modern marine phytoplankton and isotope mass balance model results (see ref. 20). The increase in fractionation of approximately +2‰ observed during the SPICE (Fig. 3) translates to a pO_2 increase from a starting point between 14–18% to a peak just over 30% (Fig. 4*A*). Use of an alternative value for J ($J = 2.5$), representing a weaker dependence of fractionation on pO_2, leads to a much larger increase in O_2 (>40%) and unrealistic O_2 volatility (including negative values) (Fig. 4*B*).

The modeled increase in O_2 using isotope mass balance during the SPICE is generally a good fit with the estimate based on increased carbon isotope fractionation (Fig. 4*A*). However, there is an apparent mismatch at the end of the SPICE (approximately 496 Ma in Fig. 4*A*) during which isotopic fractionation indicates that pO_2 returned to near pre-SPICE levels, whereas C and S isotope mass balance indicates that pO_2 remained at peak levels. This return to lower $\Delta^{13}C$ likely indicates the role that fluctuations in atmospheric pCO_2 may also play in photosynthetic carbon isotope fractionation (20, 21, 23, 26–29). Indeed, the enhanced isotopic fractionation by phytoplankton that we interpret as a response to the SPICE O_2 pulse occurred in spite of a decrease in atmospheric CO_2 brought about by the organic carbon burial that promoted the rise in O_2 (i.e., a decrease in CO_2 acting alone should lead to a decrease in fractionation) (26). Experimental results showing that isotopic fractionation in plants may be most sensitive to pO_2 at low pCO_2 and respond to changes in atmospheric pO_2/pCO_2 (refs. 21, 27) may reconcile our apparent mismatch between the isotope mass balance and fractionation approaches at the end of the SPICE.

To address the influence of changing pO_2/pCO_2 on $\Delta^{13}C$, we modeled pCO_2 during the SPICE using a modified $\delta^{13}C$ mass balance model from Kump and Arthur (26). We ran the model with constant $\Delta^{13}C$ to make no assumptions about how our measured $\Delta^{13}C$ values (Fig. 3) influence calculation of pCO_2 based on carbon sources and sinks. During the model run (see Figs. 1 and 4 for O_2), the positive $\delta^{13}C_{carb}$ excursion drives

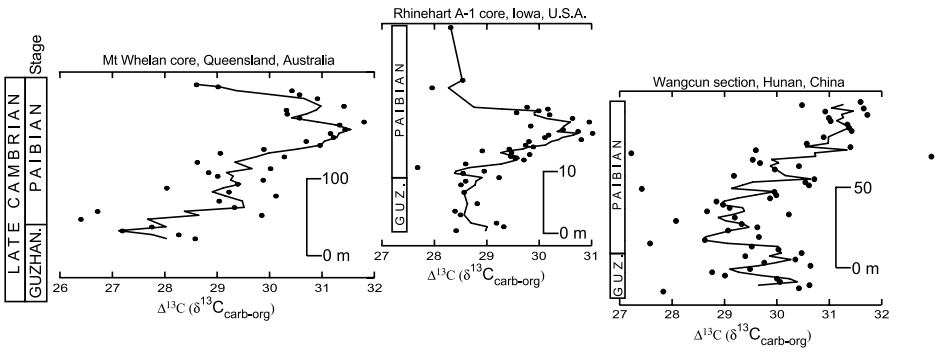

Fig. 3. Plot of $\Delta^{13}C$ ($=\delta^{13}C_{carb} - \delta^{13}C_{org}$) through the Late Cambrian based on data in Fig. 2. Line through raw data is three point running average.

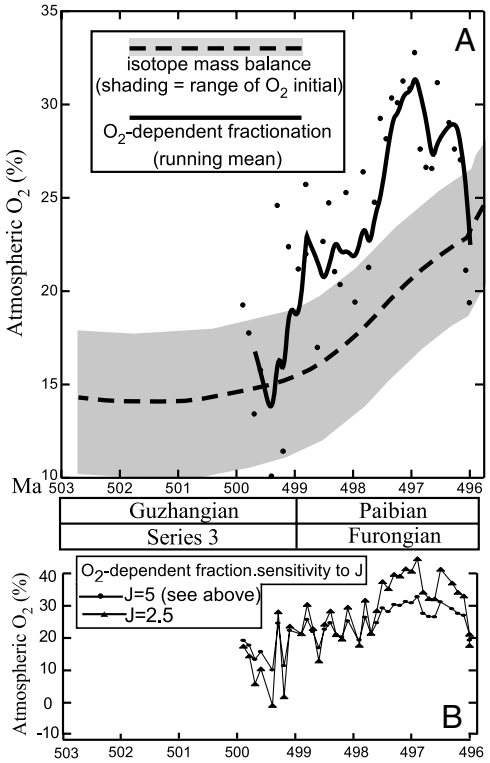

Fig. 4. (*A*) Comparison of modeled O_2 based on isotope mass balance (dashed line; shading depicts variable initial O_2 starting points shown in Fig. 1), and O_2-dependent photosynthetic fractionation (data points calculated using equation in ref. 21, and $J = 5$; see text for discussion) with solid black curve representing three point running average through the raw data. (*B*) Use of an alternative value for J ($J = 2.5$), representing a weaker dependence of fractionation on pO_2, leads to a much larger increase in O_2 (>40%) and unrealistic O_2 volatility.

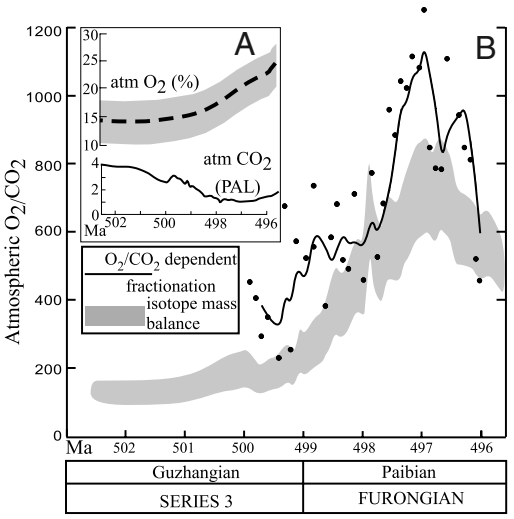

Fig. 5. (*A*) Plots of atmospheric O_2 and CO_2 through time, as modeled using isotope mass balance (see Figs. 1 and 4*A* for O_2; see text for discussion of modeling CO_2). (*B*) Plot of pO_2/CO_2 from values in Fig. 5*A* shown as shaded line (thickness of shading represents variable initial starting points for O_2 but constant initial starting point for CO_2). $\Delta^{13}C$ is used to calculate pO_2/CO_2 rather than pO_2 alone using equation 5 of Beerling et al. (21) developed for plants. Values based on photosynthetic fractionation shown as filled circles with curve representing three point running average through the raw data.

organic carbon burial rates steadily higher and atmospheric CO_2 lower during the SPICE (Fig. 5*A*) (see also curve of O_2 production due to organic C burial in Fig. 1). In response to lowered CO_2, silicate weathering decreases toward a new steady state in which the rate of volcanism (held constant throughout) is equal to the rate of silicate weathering plus the net of organic carbon burial and weathering. Then, as the perturbation to organic carbon burial that produced the SPICE is relaxed, pCO_2 rises again in the final million-year time step (Fig. 5*A*). Because pO_2 remains elevated, the curve of pO_2/pCO_2 shows a drop at this time (Fig. 5*A*, *B*) and provides a better fit to the measured changes in carbon isotope fractionation based on $\Delta^{13}C$ (Fig. 5*B*). Although this fit is good, the assumption that the experimental results performed on modern plants and bryophytes (refs. 21, 27) apply to early Paleozoic marine phytoplankton (and that they did not utilize a carbon-concentrating mechanism) must be examined further.

The observed trends in $\Delta^{13}C$ (Fig. 3) that we use as a proxy for pO_2 or pO_2/pCO_2 could also potentially record other variables that affect photosynthetic isotope discrimination (ε_p), including decreased phytoplankton growth rates, increased cell volume or changes in photoautotroph assemblages (28, 29). A global decrease in phytoplankton growth rates, however, seems at odds with the increased rates of global organic carbon and pyrite sulfur burial indicated by the SPICE (17). Whereas low oxygen conditions might have enhanced organic carbon preservation and thus burial, rather than greater burial marking increased primary production, it is unlikely that phytoplankton growth rates would decrease at three study areas at the same time, considering the wide range of depositional settings and water-mass conditions sampled. Beyond ε_p, $\Delta^{13}C$ may also incorporate changes in the temperature-dependent fractionation between dissolved inorganic carbon (DIC) and $CO_{2\,(aq)}$ in seawater and the fractionation between DIC and precipitated carbonate minerals (e.g., calcite versus aragonite) (29). However, the late Cambrian (Furongian) carbonates discussed here were deposited in relatively shallow, tropical-subtropical settings that likely experienced only relatively minor fluctuations in temperatures. Lastly, $\Delta^{13}C$ can also integrate changes in organic matter source, secondary biological fractionation (i.e., associated with heterotrophy) and/or during later burial (e.g., thermal maturation) (29). However, the sedimentary total organic carbon (TOC) in our sections is expected to be from marine sources during the later Cambrian (which predates widespread evidence for land plant megafossils), and no covariant trend is apparent in a plot of total organic carbon concentration versus $\delta^{13}C_{org}$, as might be expected if trends in individual sections were somehow artifacts of preservation (Fig S2).

Based on the above discussion, we argue that the dominant control on $\Delta^{13}C$ through the SPICE was most likely global changes in pO_2 and the pO_2/pCO_2 ratio of the Late Cambrian atmosphere and oceans. More generally, if further isotopic studies of ancient sediments (30) and additional experimental work on marine phytoplankton support the hypothesis proposed here, the results have implications for the debate surrounding usage of an appropriate negative feedback on O_2 in isotope mass balance models (19, 20). Only by allowing biological fractionation of carbon (and sulfur) isotopes to be a function of O_2 levels was Berner (19, 20) able to produce realistic O_2 fluctuations. Our results validate use of this negative feedback in O_2 mass balance models.

Implications of Oxygen Release for Biological Evolution. The significant net O_2 produced during the SPICE may have affected biological evolution over a range of timescales. In the short term, the buildup of atmospheric oxygen provided a negative feedback on the spread of anoxic waters that had resulted in a global mass extinction (and enhanced organic carbon and pyrite burial) at the onset of the SPICE (17). Indeed, the surviving shelf biota, dominated by trilobites and inarticulate brachiopods, appears to have increased in diversity at the peak of the SPICE (14).

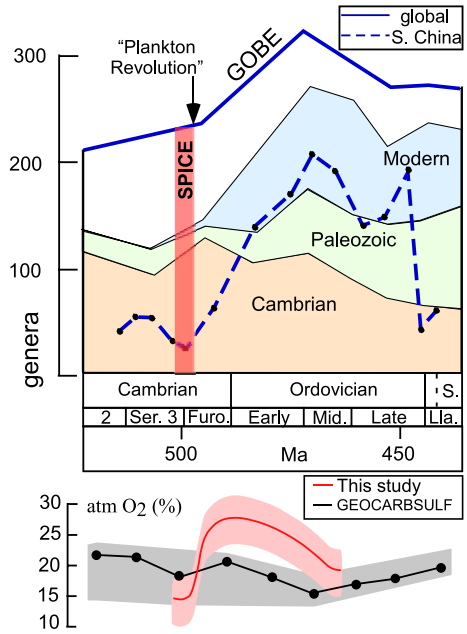

Fig. 6. Cambrian–Silurian genus level diversity from the global compilation of Alroy (36) and regional South China compilation of Rong et al. (38). Labeled are the SPICE $\delta^{13}C_{carb}$ excursion, onset of the plankton revolution (12), and the GOBE (8–10). Changes in O_2 are based on isotope mass balance model, using smoothed trends in carbon and sulfur isotopes based on compilation in the supporting online materials from Gill et al. (17). O_2 levels remain high after the SPICE organic carbon and pyrite sulfur burial event and fall through the early Ordovician, but still remain elevated above pre-SPICE levels (for comparison, GEOCARBSULF curve is modified after ref. 19).

On longer timescales, some important transitions in the plankton (12, 31, 32) and benthos (33) may have begun following the SPICE oxygenation event in the late Cambrian Furongian Series (Fig. 6).

A late Cambrian (Furongian) increase in plankton diversity is evident in the appearance of a significant number of new morphologies of organic-walled microfossils (acritarchs), including dinoflagellate-like taxa (9, 12). Although the attribution of acritarch taxa to the dinoflagellates or groups ancestral to the dinoflagellates (or any other group of eukaryotic phytoplankton) remains speculative, certain late Cambrian acritarchs share patterns of ecological and geographic distribution, organic wall chemistry, and morphologies that are comparable to those of modern dinoflagellates (7, 12). Furthermore, molecular biomarker evidence (e.g., dinosteranes) confirms that dinoflagellates were already present by the early Cambrian even if the morphological evidence is ambiguous (7, 34). Dinoflagellates, like the other modern phytoplankton that contain red algae plastids (i.e., membrane-bound organelles containing chlorophyll c as an accessory pigment), have higher quotas for trace elements that are relatively concentrated in oxygenated waters (e.g., cadmium and molybdenum) (4) compared to cyanobacteria and phytoplankton with green algae plastids. Thus, it is possible that the SPICE O_2 pulse led to an increase in oxygenated coastal ocean settings and promoted diversification of dinoflagellate-like (i.e., red plastid group) taxa relative to the prasinophyte green algae (which were members of the green plastid group, and likely the dominant producers overall throughout much of the Paleozoic; 4, 5, 7).

The latest Cambrian (Furongian) changes in the plankton included not only increased diversity but also the independent development in diverse lineages of a feeding, planktotrophic larval stage, presumably in response to more abundant food resources and predation pressures from expanding epifaunal suspension feeders (11, 31, 32). Ultimately, the SPICE oxygenation event and the beginnings of this plankton revolution (Fig. 6) may thus represent a critical initial step in the trophic chain (12) that allowed for animal groups to spread into increasingly oxygenated and ecologically diverse marine habitats during the GOBE, and become larger in size (35). Depending on the time resolution possible in recent global or regional marine animal diversity compilations (36–38), the GOBE could arguably be viewed as having been "rooted" in the latest Cambrian (Furongian) (Fig. 6). Still, because the details show that the GOBE was a multifaceted event comprised of a series of strongly diachronous biologic transitions operating on regional scales throughout the Early and Middle Ordovician (8–10, 39), no single factor would seem to suffice as an explanation. Indeed, two of the most widely recognized diversity pulses of the GOBE lag the SPICE by some approximately 25 and 35 million years (40–43) (i.e., at the Ibexian–Whiterockian boundary in North America, which is near the base of the global Dapingian Stage, and then a later event in the mid-Darriwilian).

Our isotope mass balance model indicates that atmospheric O_2 likely remained elevated for tens of millions of years after the SPICE, although the levels dropped gradually due in part to the higher rate of organic matter weathering (and marine remineralization) relative to burial (Fig. 6). If an upper bound on the H_2S concentration of an anoxic (euxinic) ocean is 1 mM (44), then a maximum of approximately 2.8×10^{18} mol O_2 was consumed as part of the negative feedback on the SPICE anoxic event, or about 15% of that produced by organic carbon and pyrite burial. The strong correspondence of the initial $\delta^{13}C$ shifts in both carbonates and organic matter at the onset of the SPICE rules out the potentially large oxygen sink associated with a dissolved organic carbon (DOC)-rich "Rothman ocean" invoked to explain Neoproterozoic carbon isotope anomalies (45). Even as O_2 levels began to drop in the early Ordovician, increasingly colder waters (42) would be capable of dissolving more atmospheric O_2 and progressively ventilating an anoxic deep ocean (46–48). Pruss et al. (46) argued that the transition to more oxic oceans drove an increase in the carbonate saturation state of surface waters that enabled the radiation of heavily skeletonized invertebrates and algae in the early Ordovician. A progressively oxygenated deep ocean should also have led to the eventual end of the recurring "biomere" extinction events that likely inhibited animal biodiversification through the later Cambrian and into the earliest parts of the Ordovician (49). Biomere extinctions have been linked to the episodic spread of anoxia into shelf environments and high rates of organic matter burial (14, 17), and therefore the termination of the biomere pattern should coincide with a period of relative stability in $\delta^{13}C_{carb}$ (50, 51) and lower organic carbon-to-phosphorus ratios in marine sediments (52). Regardless of the details, it seems likely that the late Cambrian SPICE O_2 pulse played an important role in biological evolution that continued well into the Ordovician.

Materials and Methods

Samples collected from all three sections were previously analyzed for $\delta^{13}C_{carb}$. For $\delta^{13}C_{org}$ studies here, fresh rock surfaces were generated by a water-based diamond-blade saw and the resulting thin-section billets were polished, and placed into an ultrasonic bath containing ultrapure (deionized, 18 MΩ) water to remove surficial organic contaminants. Micritic (fine-grained) components were microdrilled (approximately 1.5 g of powder) from the thin-section billets. Sample powders were accurately weighed and thoroughly acidified using approximately 6N HCl to remove carbonate minerals. Insoluble fractions were then repeatedly rinsed in ultrapure water and dried at 85 °C. Remaining residues were weighed and homogenized, and then loaded into tin capsules. Samples were combusted with a Costech Elemental Analyzer and the resulting CO_2 gas analyzed for $\delta^{13}C$ through a Finnigan Delta IV stable isotope ratio mass spectrometer under continuous flow using an open-split CONFLO III interface in the Stable Isotope Biogeochemistry Laboratory at The Ohio State University. Carbon isotope ratios presented here are reported in per mil notation relative to the Vienna Peedee Belmenite limestone standard [‰ Vienna Peedee Belemnite standard

(VPDB)]. Repeated measurements of the IAEA-CH7 standards were ±0.15‰ for $\delta^{13}C$ and ±1.0% for %C (1 standard deviation). Weight percent of TOC in samples is determined by comparison of voltages for the ion beam intensities of masses 44, 45, and 46 CO_2^+ between our samples and known wt. % carbon of the gravimetric standard Acetanilide.

ACKNOWLEDGMENTS. We thank three anonymous reviewers for constructive comments. We thank R. McKay at the Iowa Geol. Survey for sample access; J. Gouldey for sample preparation; A. H. Knoll for discussion; and Y. Matsui and A. Grottoli at The Ohio State University Stable Isotope Laboratory for analytical support. This work was supported by the National Science Foundation Geobiology and Low Temperature Geochemistry program.

1. Berner RA, Vandenbrooks JM, Ward PD (2007) Oxygen and evolution. *Science* 316:557–558.
2. Anbar AD, Knoll AH (2002) Proterozoic ocean chemistry and evolution: A bioinorganic bridge? *Science* 297:1137–1142.
3. Canfield DE, Poulton SW, Narbonne GM (2007) Late Neoproterozoic deep-ocean oxygenation and the rise of animal life. *Science* 315:92–95.
4. Falkowski P, et al. (2004) The evolution of modern eukaryotic phytoplankton. *Science* 305:354–360.
5. Payne JL, van de Schootbrugge B (2007) *Evolution of Primary Producers in the Sea*, eds PG Falkowski and AH Knoll (Elsevier, London), pp 165–189.
6. Butterfield NJ (1997) Plankton ecology and the Proterozoic–Phanerozoic transition. *Paleobiology* 23:247–262.
7. Knoll AH, Summons RE, Waldbauer JR, Zumberge JE (2007) *Evolution of Primary Producers in the Sea*, eds PG Falkowski and AH Knoll (Elsevier, London), pp 133–163.
8. Webby BD, Paris F, Droser ML, Percival IG (2004) *The Great Ordovician Biodiversification Event* (Columbia University Press, New York).
9. Servais T, et al. (2010) The Great Ordovician Biodiversification Event (GOBE): The palaeoecological dimension. *Palaeogeogr Palaeocl* 294:99–119.
10. Miller AI, Foote M (1996) Calibrating the Ordovician Radiation of marine life: Implications for Phanerozoic diversity trends. *Paleobiology* 22:304–309.
11. Signor PW, Vermeij GJ (1994) The plankton and the benthos: Origins and early history of an evolving relationship. *Paleobiology* 20:297–319.
12. Servais T, et al. (2008) Ordovician Biodiversification: Revolution in the oceanic trophic chain. *Lethaia* 41:99–109.
13. Miller AI, Mao S (1995) Association of orogenic activity with the Ordovician radiation of marine life. *Geology* 23:305–308.
14. Saltzman MR, et al. (2000) A global carbon isotope excursion (SPICE) during the Late Cambrian: relation to trilobite extinctions, organic-matter burial and sea level. *Palaeogeogr Palaeocl* 162:211–223.
15. Ahlberg P, et al. (2009) Cambrian high-resolution biostratigraphy and carbon isotope chemostratigraphy in Scania, Sweden: First record of the SPICE and DICE excursions in Scandinavia. *Lethaia* 42:2–16.
16. Kouchinsky A, et al. (2008) The SPICE carbon isotope excursion in Siberia: A combined study of the upper Middle Cambrian–lowermost Ordovician Kulyumbe River section, northwestern Siberian Platform. *Geol Mag* 145:609–622.
17. Gill BC, et al. (2011) Geochemical evidence for widespread euxinia in the Later Cambrian ocean. *Nature* 469:80–83.
18. Kump LR, Garrels RM (1986) Modeling atmospheric O_2 in the global sedimentary redox cycle. *Am J Sci* 286:337–360.
19. Berner RA (2006) GEOCARBSULF: A combined model for Phanerozoic atmospheric O_2 and CO_2. *Geochim Cosmochim Acta* 70:5653–5664.
20. Berner RA, et al. (2000) Isotope fractionation and atmospheric oxygen: Implications for Phanerozoic O_2 evolution. *Science* 287:1630–1633.
21. Beerling DJ, et al. (2002) Carbon isotope evidence implying high O_2/CO_2 ratios in the Permo-Carboniferous atmosphere. *Geochim Cosmochim Acta* 66:3757–3767.
22. Kurtz AC, Kump LR, Arthur MA, Zachos JC, Paytan A (2003) Early Cenozoic decoupling of the global carbon and sulfur cycles. *Paleoceanography* 18:1090.
23. Bergman NM, Lenton TM, Watson AJ (2004) COPSE: A new model of biogeochemical cycling over Phanerozoic time. *Am J Sci* 304:397–437.
24. Dahl TW, et al. (2010) Devonian rise in atmospheric oxygen correlated to the radiations of terrestrial plants and large predatory fish. *Proc Natl Acad Sci USA* 107:17911–17915.
25. Saltzman MR, et al. (2004) The Late Cambrian SPICE ($\delta^{13}C$) event and the Sauk II-Sauk III regression: New evidence from Laurentian basins in Utah, Iowa, and Newfoundland. *J Sediment Res* 74:366–377.
26. Kump LR, Arthur MA (1999) Interpreting carbon-isotope excursions: Carbonates and organic matter. *Chem Geol* 161:181–198.
27. Fletcher BJ, Brentnall SJ, Quick WP, Beerling DJ (2006) BRYOCARB: A process-based model of thallose liverwort carbon isotope fractionation in response to CO_2, O_2, light and temperature. *Geochim Cosmochim Acta* 70:5676–5691.
28. Popp BM, et al. (1998) Effect of phytoplankton cell geometry on carbon isotopic fractionation. *Geochim Cosmochim Acta* 62:69–77.
29. Hayes JM, Strauss H, Kaufman AJ (1999) The abundance of ^{13}C in marine organic matter and isotopic fractionation in the global biogeochemical cycle of carbon during the past 800 Ma. *Chem Geol* 161:103–125.
30. Baker JL, Jiang G, Zeiza A (2010) Carbon isotopic fractionation across a Late Cambrian carbonate platform: A regional response to the SPICE event as recorded in the Great Basin, western United States. *Geol Soc Amer Abs* 42:44.
31. Petersen KJ (2005) Macroevolutionary interplay between planktic larvae and benthic predators. *Geology* 33:929–932.
32. Nützel AO, Lehnert O, Fryda J (2006) Origin of planktotrophy—Evidence from early molluscs. *Evol Dev* 8:325–330.
33. Nardin E, Lefebvre B (2010) Unraveling extrinsic and intrinsic factors of the early Palaeozoic diversification of blastozoan echinoderms. *Palaeogeogr Palaeocl* 294:142–160.
34. Moldowan JM, Talyzina NM (1998) Biogeochemical evidence for dinoflagellate ancestors in the Early Cambrian. *Science* 281:1168–1170.
35. Payne JL, Finnegan S (2006) Controls on marine animal biomass through geological time. *Geobiology* 4:1–10.
36. Alroy J (2010) The shifting balance of diversity among major marine animal groups. *Science* 329:1191–1194.
37. Sepkoski JJ (1997) Biodiversity: Past, present, and future. *J Paleo* 71:533–539.
38. Rong J, Junxuan F, Miller AI, Guoxiang L (2007) Dynamic patterns of latest Proterozoic-Palaeozoic-early Mesozoic marine biodiversity in South China. *Geol J* 42:431–454.
39. Zhan R, Harper DAT (2006) Biotic diachroneity during the Ordovician Radiation: Evidence from South China. *Lethaia* 39:211–226.
40. Droser ML, Finnegan S (2003) The Ordovician Radiation: A follow-up to the Cambrian Explosion? *Integr Comp Biol* 43:178–184.
41. Droser ML, Sheehan PM (1997) Palaeoecology of the Ordovician Radiation: resolution of large-scale patterns with individual clade histories, palaeogeography and environments. *Geobios* 20:221–229.
42. Trotter JA, Williams IA, Barnes CR, Lecuyer C, Nicoll RS (2008) Did cooling oceans trigger Ordovician biodiversification? Evidence from conodont thermometry. *Science* 321:550–554.
43. Schmitz B, et al. (2008) Asteroid breakup linked to the Great Ordovician Biodiversification Event. *Nat Geosci* 1:49–53.
44. Meyer KM, Kump LR, Ridgwell A (2008) Biogeochemical controls on photic-zone euxinia during the end-Permian mass extinction. *Geology* 36:747–750.
45. Rothman DH, Hayes JM, Summons RE (2003) Dymanics of the Neoproterozoic carbon cycle. *Proc Natl Acad Sci USA* 100:8124–8129.
46. Pruss SB, Finnegan S, Fischer WW, Knoll AH (2010) Carbonates in skeleton-poor seas: New insights from Cambrian and Ordovician strata of Laurentia. *Palaios* 25:73–84.
47. Hurtgen MT, Pruss SB, Knoll AH (2009) Evaluating the relationship between the carbon and sulfur cycles in the later Cambrian ocean: An example from the Port au Port group, western Newfoundland, Canada. *Earth Planet Sc Lett* 281:288–297.
48. Berry WBN, Wilde P (1978) Progressive ventilation of the oceans—An explanation for the distribution of the lower Paleozoic black shales. *Am J Sci* 278:257–275.
49. Bambach R, Knoll AH, Wang S (2004) Origination, extinction, and mass depletions of marine diversity. *Paleobiology* 30:522–542.
50. Saltzman MR (2005) Phosphorus, nitrogen, and the redox evolution of the Paleozoic oceans. *Geology* 33:573–576.
51. Munnecke A, Calner M, Harper DAT, Servais T (2010) Ordovician and Silurian sea-water chemistry, sea level, and climate: A synopsis. *Palaeogeogr Palaeocl* 296:389–413.
52. Algeo TJ, Ingall E (2007) Sedimentary Corg: P ratios, paleocean ventilation, and Phanerozoic atmospheric pO_2. *Palaeogeogr Palaeocl* 256:130–155.